Electronic Absorption Spectra of Neutral Perylene ($C_{20}H_{12}$), Terrylene ($C_{30}H_{16}$), and Quaterrylene ($C_{40}H_{20}$) and Their Positive and Negative Ions: Ne Matrix-Isolation Spectroscopy and Time-Dependent Density Functional Theory Calculations

Thomas M. Halasinski,[†,§] Jennifer L. Weisman,[#] Richard Ruiterkamp,[⊥] Timothy J. Lee,[||] Farid Salama,*[,†] and Martin Head-Gordon[#]

Space Science Division, NASA Ames Research Center, Mail Stop 245-6, Moffett Field, California 94035, Department of Chemistry, University of California, Berkeley, and Chemical Sciences Division, Lawrence Berkeley National Laboratory, Berkeley, California 94720, Raymond & Beverly Sackler Laboratory at Leiden Observatory, P.O. Box 9513, 2300 RA Leiden, The Netherlands, and NASA Advanced Supercomputing Division, NASA Ames Research Center, Mail Stop 230-3, Moffett Field, California 94035

Received: November 5, 2002; In Final Form: February 19, 2003

We present an experimental and theoretical study of an interesting series of polycyclic aromatic hydrocarbons, the oligorylenes. The absorption spectra of perylene, terrylene, and quaterrylene in neutral, cationic, and anionic charge states are obtained by matrix-isolation spectroscopy in Ne. The experimental spectra are dominated by a bright state that red shifts with growing molecular size. Excitation energies and state symmetry assignments for this state are obtained by calculations using time-dependent density functional theory methods. These calculations also provide additional information and insight into the trends in oscillator strength and excitation energy for the bright states: in particular, the oscillator strength per unit mass of carbon increases along the series.

I. Introduction

Polycyclic aromatic hydrocarbons (PAHs) are now thought to be ubiquitous throughout the interstellar medium on the basis of the detection of their widespread infrared spectral signature.[1] PAHs are also attractive candidates for (some of) the diffuse interstellar bands (DIBs), visible absorption features that are associated with low-density regions of interstellar space.[2] In space, PAH molecules are present as neutral, positively charged, and negatively charged species. The charge distribution varies with the physical conditions (interstellar field, electron density, and temperature, etc.) that reign in the various regions of the interstellar medium.[2] The comparison of the infrared signatures of PAHs in laboratory spectra with that of the astronomical data suggests that one class of molecules responsible for the interstellar emission features are PAHs. More specific information would result, however, from the detection of the electronic/vibronic signature of interstellar PAHs. Thus, the best prospect in detecting individual PAH molecules in the interstellar medium lies in the identification of the origin of the DIBs.

Current experimental research is directed toward extending the size,[3] structure,[4] and charge state[5] distributions of the molecules studied in the laboratory. Matrix-isolation spectroscopy experiments offer a crucial guideline for future laboratory studies by allowing the preselection of promising PAH molecules to be studied in free jet expansions. Definitive tests of the proposal that PAH ions are responsible for some of the DIBs must await the availability of laboratory measurements of the free molecules and ions in the gas phase that are still not available for molecules as large as terrylene and quaterrylene presented in this study.

Theoretical calculations are a valuable tool to guide and support current and future laboratory studies. Time-dependent density functional theory methods[6] are capable of producing reasonably accurate vertical excitation energies and oscillator strengths for large systems. For example, in studies of naphthalene, perylene, and pyrene radical cations,[7] accuracies of approximately ±0.3 eV were found for excitation energies. In addition to simply predicting absorption spectra, it is possible to gain insight into the nature of the absorptions and more easily extract trends that may aid in the direction of future investigations as illustrated in the current study of perylene, terrylene, and quaterrylene.

The collection and analysis of the spectra of these species contribute to a spectral database upon which to identify possible candidates for the DIBs, as well as information concerning the photophysical processes of absorption and emission of radiation within the interstellar medium. Ultimately, through studies such as this, a more complete understanding of the physical conditions and the chemical evolution within the interstellar medium can be reached.

In a parallel paper,[3] we discuss the astrophysical implications of the spectroscopy of a large set of neutral and ionized PAHs. Here, we discuss the detailed analysis of the electronic spectra of a subset of the original set, namely, the oligorylenes perylene, terrylene, and quaterrylene, that present interesting spectroscopic properties. Matrix-isolated spectra and supporting time-dependent density functional theory (TDDFT) calculations are presented for these large molecular systems.

* To whom correspondence should be addressed. E-mail: fsalama@mail.arc.nasa.gov.

[†] Space Science Division, NASA Ames Research Center.

[§] Present address: Department of Chemistry, Saint Joseph's University, Philadelphia, PA 19131.

[#] University of California, Berkeley, and Lawrence Berkeley National Laboratory.

[⊥] Raymond & Beverly Sackler Laboratory at Leiden Observatory.

[||] NASA Advanced Supercomputing Division, NASA Ames Research Center.

10.1021/jp027394w CCC: $25.00
Published on Web 04/12/2003

II. Methods

II.a. Experimental Methods. The experimental instrumentation employed in these studies, a UV/visible/near-IR spectrometer equipped with its own dedicated sample vacuum chamber and matrix deposition source, has been previously described.[8] A brief review will be given here. The UV/visible/near-IR instrument is equipped with a sapphire sample window cooled to 4.2 K by an extended liquid helium transfer cryostat. The sample window can be rotated 360° under vacuum to face, alternatively, two spectroscopic window ports, the matrix gas and PAH deposition lines, and a MgF_2 VUV window port.

Single beam spectra of the cold substrate were collected before the matrix was deposited and used as the background for all spectra reported unless noted otherwise. A deuterium lamp provides spectral output from 160 to 360 nm, and a quartz tungsten halogen lamp provides output from 320 to 2500 nm. Spectra were recorded from 180 to 1000 nm with a nominal resolution of 0.1 nm.

The vaporization and codeposition of each PAH with the inert gas (neon) was performed using Pyrex tubes (12.7 mm o.d.), which were mounted on the sample chamber through stainless steel Cajon Ultratorr fittings and heated from outside the vacuum chamber with the use of heating tape. The tubes were positioned between 4 and 5 cm from the cold window and perpendicular to the surface of the cold substrate. The temperature of the tube was monitored using a chromel/alumel thermocouple mounted on the exterior of each tube with Al foil tape.

Matrix gas was admitted through a port at a position 45° from the plane of the substrate surface and the median between the Pyrex tube containing the PAH sample such that the two vapor streams combined before the surface of the window. Typical deposition temperatures for each PAH were 108, 260, and 396 °C for perylene, terrylene, and quaterrylene, respectively. Ne flow rates were estimated to be 12 mmol/h. Based on these flow rates and vaporization temperatures, the matrix/PAH ratio is estimated to be in excess of 1000/1. Typical deposition times varied from 2 to 4 h. Matrices used with NO_2 as an electron acceptor were formed by deposition of premixed 1000/1 Ne/NO_2 gas samples.

A microwave-powered, hydrogen flow (10% H_2/He) discharge lamp (Opthos Instruments MPG 4M) mounted on the MgF_2 vacuum chamber window was used for photolysis of the matrix. This lamp generates nearly monochromatic radiation in the Lyman α line at 121.6 nm (10.2 eV). Typical photolysis times ranged from 2 to 20 min.

Perylene (99.5+%) and NO_2 (99.5+%) were obtained from Aldrich Chemical Co. The terrylene and quaterrylene samples were obtained from Dr. W. Schmidt (PAH Forschungs Institut, Greifenberg, Germany). Ne (Cryogenic Rare Gas 99.9995%) research-grade rare gas was the inert matrix material utilized in the experimental studies. All chemicals were used as received.

II.b. Computational Methods. The ground-state structures of perylene, terrylene, and quaterrylene were optimized using Kohn−Sham density functional theory (DFT) with the Becke exchange functional,[9] the LYP correlation functional,[10] and the 6-31G* basis set. The neutral, radical cation, and radical anion charge states of the three molecules were each optimized at the BLYP/6-31G* level. Time-dependent density functional theory (TDDFT) methods were used to determine the absorption spectra of the molecules. The DFT and TDDFT calculations were implemented in the Q-Chem program package.[11]

TDDFT vertical excitation energies are generally insensitive to basis set size (for a representative example, see ref 7). We performed a study of the perylene excitation energies in the three charge states to verify the lack of basis set dependence. We found that small basis sets were sufficient to accurately describe the strongest visible excitation for these species (these data are available in Table 1 of Supporting Information). The neutral and radical cation TDDFT calculations were performed at the BLYP/6-31G//BLYP/6-31G* level, while the radical anion calculations were performed at the BLYP/6-31G*//BLYP/6-31G* level, where the "double slash" notation means "at the geometry of".

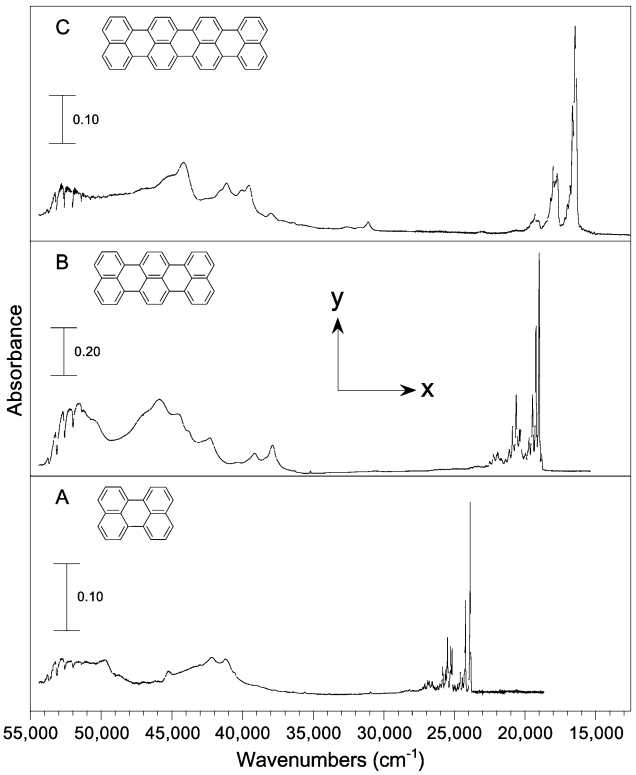

Figure 1. The UV/visible spectra of a codeposit of (A) a 10 min deposit of perylene in Ne, (B) a 10 min deposit of terrylene in Ne, and (C) a 40 min deposit of quaterrylene in Ne. The molecular axis chosen for the symmetries of the molecular orbitals and electronic states of all three PAHs is given in the inset.

III. Results and Discussion

III.a. Experimental Results. The absorption spectra of neutral perylene, terrylene, and quaterrylene from 13 000 to 55 000 cm^{-1} (180−770 nm) are shown in Figure 1. The most structured absorption band system in all three cases belongs to the transition from the ground electronic state to the first excited electronic state. This transition shifts to the red as the molecular size increases in the series. Several vibronic bands are observed in the first excited state for all three molecules (expanded views of the three spectra are shown in Figure 2). The fwhm of the observed vibronic bands also increase with molecular size. Several higher-lying excited electronic states are also observed for each molecule. It is not clear whether they follow similar trends with molecular size because their spectral assignments are uncertain.

The matrix-isolated samples containing NO_2-doped Ne were subjected to Lyman α (10.2 eV) photolysis. NO_2 was added to the matrix gas to act as an electron acceptor, facilitating the formation of PAH cations by inhibiting the formation of the counterions (PAH anions). The spectral features that grew upon

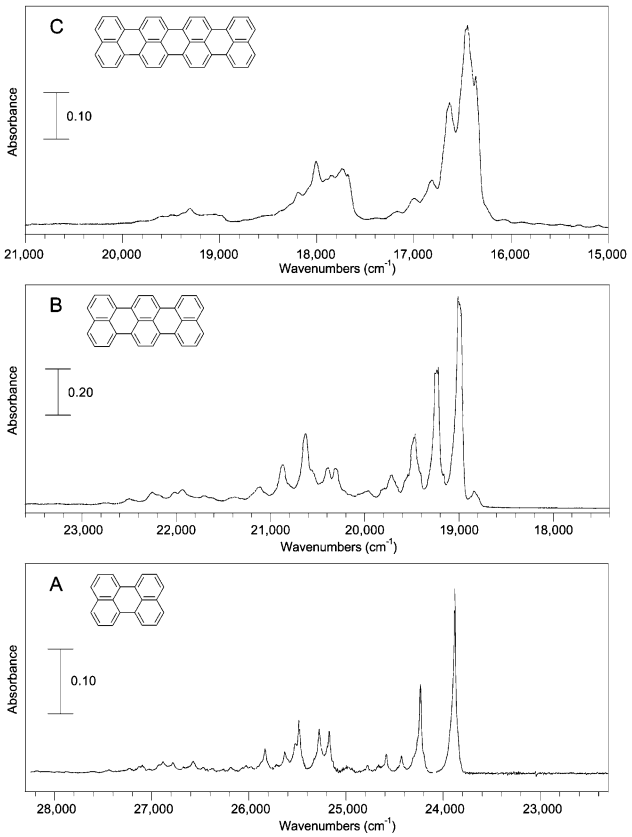

Figure 2. Expanded regions of the spectra shown in Figure 1.

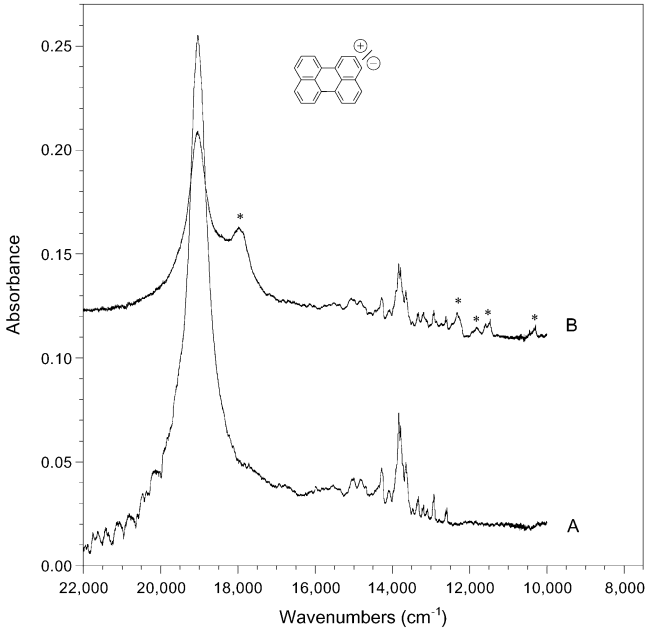

Figure 3. The visible/near-IR spectra of (A) a 3 h deposit of perylene and NO_2 in Ne followed by 10 min of Lyman α photolysis and (B) a 3 h deposit of perylene in Ne followed by 10 min of Lyman α photolysis. The spectral features denoted with an asterisk have been assigned to the perylene anion.

photolysis for perylene, terrylene, and quaterrylene are shown in the difference spectra obtained by subtracting the measured absorbance of the sample before photolysis from the measured absorbance of the sample after photolysis (Figures 3A, 4A, and 5A, respectively). A single intense absorption is observed in each case that shifts to the red as the molecular size increases in the series.

The difference spectra of matrix samples photolyzed in the absence of NO_2 for perylene, terrylene, and quaterrylene are given in Figures 3B, 4B, and 5B, respectively. Similar to the spectral features of the PAH cations for this series of molecules, the spectral features of the PAH anions are dominated by a single intense absorption feature that shifts to the red as the molecular size increases in the series. We discuss below each individual spectrum.

III.a.i. Perylene ($C_{20}H_{12}$). Several studies of the electronic absorption spectra of perylene isolated in noble gas matrices have been reported previously.[12] The spectral properties are reported here for comparison purposes with the spectra of neutral terrylene and quaterrylene. In addition, we report new calculations for the first excited electronic state. The chosen molecular axis, illustrated in Figure 1, has the molecule lying in the *xy* plane, *x* being the long axis of the molecule.

Figure 1A displays the electronic absorption spectrum of neutral perylene from 19 000 to 55 000 cm^{-1} (180−530 nm). The observed band positions and associated vibrational spacings are available in Table 2 of Supporting Information. The transition from the ground electronic state to the first excited state has been assigned (e.g., see ref 12b and references therein) to involve a $S_1(B_{3u}) \leftarrow S_0(A_g)$ transition. Two series of bands were observed for the $S_1(B_{3u}) \leftarrow S_0(A_g)$ transition by Joblin et al. and were assigned as isolated perylene trapped in two different sites in Ne matrices (site a and site b). The full progression of site a is listed in this report, we only list the vibronic origin of site b at 39 cm^{-1} to the red of the vibronic origin of site a.

An expanded view of the 23 000 to 28 000 cm^{-1} (360−430 nm) region is illustrated in Figure 2A. Only a few fundamental vibrational modes (348, 543, 1098, 1293, 1395, and 1601 cm^{-1}) are responsible for the majority of observed vibronic bands in the $S_1(B_{3u}) \leftarrow S_0(A_g)$ transition. Several spectral features due to vibronic progressions in higher electronic states are also observed in Figure 1 and listed in Table 2 of Supporting Information.

Figure 3A displays the spectral features produced upon photolysis of perylene isolated in a Ne matrix doped with NO_2 and assigned to the perylene cation.[7,13] The positions of the observed bands are listed in Table 3 of Supporting Information along with assignments from Hirata et al.[7] The majority of the observed bands in the perylene cation show a multicomponent splitting. This splitting has been assigned to the presence of different sites within the solid matrix or to transitions involving low vibrational frequencies of the perylene cation.[12b]

Figure 3B displays the spectral features produced upon photolysis of perylene isolated in a Ne matrix (in the absence of NO_2). The bands that are observed in this spectrum and are absent or very weak in Figure 3A are denoted with an asterisk and assigned to the perylene anion. The positions of the observed bands assigned to the perylene anion are listed in Table 4 of Supporting Information. Multicomponent splitting is observed in the majority of perylene anion bands that are similar in nature to those observed in the perylene cation. Discussion of the assignments for some of the stronger bands is given in section III.b.

III.a.ii. Terrylene ($C_{30}H_{16}$). Figure 1B displays the electronic absorption spectrum of neutral terrylene from 16 000 to 55 000 cm^{-1} (180−630 nm), and Table 5 of Supporting Information lists the observed band positions and associated vibrational spacings. An expanded view of the 18 000 to 23 000 cm^{-1} (430−560 nm) region is illustrated in Figure 2B. Similar to the perylene cation, we assign the spectral feature to the red of the

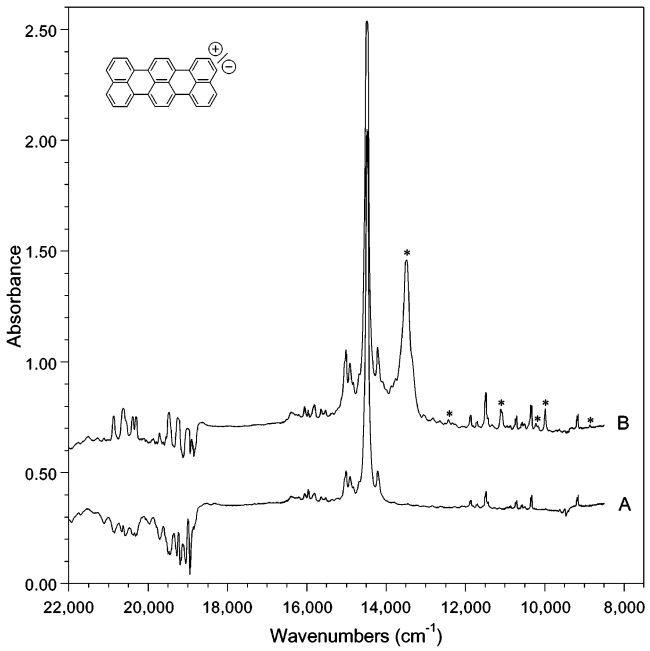

Figure 4. The visible/near-IR spectra of (A) a 3 h deposit of terrylene and NO_2 in Ne followed by 10 min of Lyman α photolysis and (B) a 3 h deposit of terrylene in Ne followed by 10 min of Lyman α photolysis. The spectral features denoted with an asterisk have been assigned to the terrylene anion.

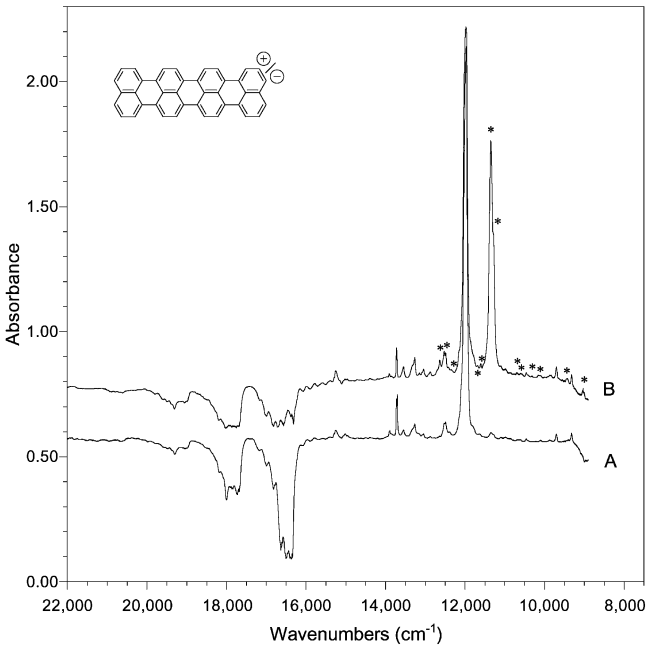

Figure 5. The visible/near-IR spectra of (A) a 3 h deposit of quaterrylene and NO_2 in Ne followed by 10 min of Lyman α photolysis and (B) a 3 h deposit of quaterrylene in Ne followed by 10 min of Lyman α photolysis. The spectral features denoted with an asterisk have been assigned to the quaterrylene anion.

main vibronic origin as a site splitting. The larger 154 cm^{-1} shift compared to the 39 cm^{-1} shift of the perylene cation presumably arises from the larger size of the molecular ion. Also similar to neutral perylene, only a few fundamental vibrational modes (241, 1311, 1398, and 1634 cm^{-1}) are responsible for the vibronic progression observed in the $S_1(B_{3u}) \leftarrow S_0(A_g)$ transition of neutral terrylene. These features are in good agreement with the spectral features observed at 247, 1317, 1390, and 1590 cm^{-1} by fluorescence excitation of terrylene in Ne matrices.[14]

Figure 4A displays the spectral features produced upon photolysis of terrylene isolated in a Ne matrix doped with NO_2, which we assign to the terrylene cation. The positions of the observed bands are listed in Table 6 of Supporting Information. The majority of bands observed in the terrylene cation show a splitting into multicomponents. We assign the origin of this splitting to a similar site effect responsible for the multicomponents observed in the spectral features for the perylene cation and anion.

Figure 4B displays the spectral features produced upon photolysis of terrylene isolated in a Ne matrix (in the absence of NO_2). The bands that are observed in this spectrum and are absent or very weak in Figure 4A are denoted with an asterisk and assigned to the terrylene anion. The positions of the observed bands assigned to the terrylene anion are listed in Table 7 of Supporting Information. Splitting of the spectral features into multicomponents is also observed in this molecular radical. Discussion of the assignments for the strongest bands observed in the spectra of the terrylene cation and anion is given in section III.b.

III.a.iii. Quaterrylene ($C_{40}H_{20}$). Figure 1C displays the electronic absorption spectrum of neutral quaterrylene from 13 000 to 55 000 cm^{-1} (180−770 nm), and Table 8 of Supporting Information lists the observed band positions and associated vibrational spacings. An expanded view of the 15 000 to 21 000 cm^{-1} (480−670 nm) region is illustrated in Figure 2C. Comparison of the spectra in Figure 2A−C shows that the observed spectral features appear to broaden with increasing molecular size. While neutral perylene and neutral terrylene have one spectral feature each that we assign to site splittings, neutral quaterrylene has at least two spectral features lying 89 and 373 cm^{-1} to the red of the most intense transition that may also be assigned to site effects. Also similar to neutral perylene and terrylene, only a few fundamental vibrational modes (186, 1281, 1395, and 1555 cm^{-1}) are responsible for the vibronic progression observed in the $S_1(B_{3u}) \leftarrow S_0(A_g)$ transition of neutral quaterrylene.

Figure 5A displays the spectral features produced upon photolysis of quaterrylene isolated in a Ne matrix doped with NO_2, which we assign to the quaterrylene cation. The positions of the observed bands are listed in Table 9 of Supporting Information. Unlike the perylene cation/anion and the terrylene cation/anion, the quaterrylene cation does not exhibit multicomponents to individual spectral bands. Presumably, this is due to the observed increased broadening of the spectral features with molecular size.

Figure 5B displays the spectral features produced upon photolysis of quaterrylene isolated in a Ne matrix (in the absence of NO_2). The bands that are observed in this spectrum and are absent or very weak in Figure 5A are denoted with an asterisk and assigned to the quaterrylene anion. The positions of the observed bands assigned to the quaterrylene anion are listed in Table 10 of Supporting Information. As with the quaterrylene cation, splitting of the spectral features into multicomponents is not observed. Discussion of the assignments for the strongest feature observed in the spectra of the quaterrylene cation and anion is given in section III.b.

Comparison of the relative spectral intensities for the most intense transition observed for the radical species of perylene, terrylene, and quaterrylene in Figures 3−5 suggests that this transition increases in intensity with molecular size. We discuss below a computational argument for this observation.

III.b. Computational Results. The calculated TDDFT absorption spectra for the three molecules in three charge states

TABLE 1: Perylene Calculated TDDFT Absorption Spectrum

transition symmetry	state assignment	TDDFT exc. energy (eV)	TDDFT osc. strength	exptl. energy eV	exptl. energy cm^{-1}
		Neutral			
B_{3u}	$^1A_g \rightarrow {}^1B_{3u}$	2.6414	0.3088	2.96	23 883
B_{2u}	$^1A_g \rightarrow {}^1B_{2u}$	3.6432	0.0047		
B_{2u}	$^1A_g \rightarrow {}^1B_{2u}$	4.3002	0.1015		
B_{3u}	$^1A_g \rightarrow {}^1B_{3u}$	4.9603	0.0293		
B_{3u}	$^1A_g \rightarrow {}^1B_{3u}$	4.9693	0.0025		
		Radical Cation			
B_{2u}	$^2A_u \rightarrow {}^2B_{2g}$	1.6246	0.0002		
B_{3u}	$^2A_u \rightarrow {}^2B_{3g}$	1.6831	0.0001		
B_{2u}	$^2A_u \rightarrow {}^2B_{2g}$	1.9174	0.0288		
B_{3u}	$^2A_u \rightarrow {}^2B_{3g}$	2.4389	0.3481	2.36	19 036
		Radical Anion			
B_{2u}	$^2B_{3g} \rightarrow {}^2B_{1u}$	1.3930	0.0040		
B_{3u}	$^2B_{3g} \rightarrow {}^2A_u$	1.6065	0.0025		
B_{2u}	$^2B_{3g} \rightarrow {}^2B_{1u}$	1.6399	0.0347		
B_{1u}	$^2B_{3g} \rightarrow {}^2B_{2u}$	1.7335	0.0028		
B_{3u}	$^2B_{3g} \rightarrow {}^2A_u$	2.2555	0.3328	2.23	17 976

TABLE 2: Terrylene Calculated TDDFT Absorption Spectrum

transition symmetry	state assignment	TDDFT exc. energy (eV)	TDDFT osc. strength	exptl. energy eV	exptl. energy cm^{-1}
		Neutral			
B_{3u}	$^1A_g \rightarrow {}^1B_{3u}$	2.0211	0.6734	2.35	18 993
B_{2u}	$^1A_g \rightarrow {}^1B_{2u}$	2.9852	0.0001		
B_{2u}	$^1A_g \rightarrow {}^1B_{2u}$	3.3190	0.0075		
B_{2u}	$^1A_g \rightarrow {}^1B_{2u}$	3.4078	0.0046		
B_{3u}	$^1A_g \rightarrow {}^1B_{3u}$	3.8441	0.0116		
		Radical Cation			
B_{3u}	$^2A_u \rightarrow {}^2B_{3g}$	1.1723	0.0012		
B_{2u}	$^2A_u \rightarrow {}^2B_{2g}$	1.8247	0.0144		
B_{2u}	$^2A_u \rightarrow {}^2B_{2g}$	1.9143	0.0107		
B_{3u}	$^2A_u \rightarrow {}^2B_{3g}$	1.9257	0.7056	1.80	14 478
		Radical Anion			
B_{3u}	$^2B_{3g} \rightarrow {}^2A_u$	1.1026	0.0053		
B_{2u}	$^2B_{3g} \rightarrow {}^2B_{1u}$	1.5941	0.0287		
B_{3u}	$^2B_{3g} \rightarrow {}^2A_u$	1.7626	0.6052	1.67	13 486
B_{2u}	$^2B_{3g} \rightarrow {}^2B_{1u}$	1.8424	0.0038		
B_{1u}	$^2B_{3g} \rightarrow {}^2B_{2u}$	2.0948	0.0030		

are presented in Tables 1 (perylene), 2 (terrylene), and 3 (quaterrylene), along with the experimental absorptions that may be matched with the TDDFT results. The lowest several calculated states that are symmetry-allowed are presented for each species. The vertical TDDFT excitation energies are given in electronvolts, along with the oscillator strength and symmetry of the transition. Perylene, terrylene, and quaterrylene all belong to the D_{2h} molecular symmetry point group and the ground-state symmetries of each neutral, radical cation, and radical anion are ^1A_g, ^2A_u, and $^2B_{3g}$, respectively. The transition symmetries are assigned on the basis of the molecule lying in the *xy* plane, *x* being the long axis of the molecule.

The results are discussed as follows. The strong dominant absorption for each molecule is considered in a section on bright states (bright states in our specific context are electronically dipole-allowed transitions). We hereafter use the term bright state to refer to the strong excitation in each spectrum. We next discuss the trends observed and explain the origin of these trends. Finally, we consider the astrophysical implications of these bright states in terms of qualitative trends of the excitation energies and oscillator strengths in another section.

TABLE 3: Quaterrylene Calculated TDDFT Absorption Spectrum

transition symmetry	state assignment	TDDFT exc. energy (eV)	TDDFT osc. strength	exptl. energy eV	exptl. energy cm^{-1}
		Neutral			
B_{3u}	$^1A_g \rightarrow {}^1B_{3u}$	1.6730	1.0792	2.04	16 453
B_{3u}	$^1A_g \rightarrow {}^1B_{3u}$	2.9730	0.0118		
B_{2u}	$^1A_g \rightarrow {}^1B_{2u}$	3.1382	0.0038		
B_{2u}	$^1A_g \rightarrow {}^1B_{2u}$	3.2509	0.0093		
B_{2u}	$^1A_g \rightarrow {}^1B_{2u}$	3.4006	0.0012		
		Radical Cation			
B_{3u}	$^2A_u \rightarrow {}^2B_{3g}$	0.8930	0.0043		
B_{3u}	$^2A_u \rightarrow {}^2B_{3g}$	1.6188	1.0277	1.48	11 975
B_{2u}	$^2A_u \rightarrow {}^2B_{2g}$	1.8067	0.0182		
B_{2u}	$^2A_u \rightarrow {}^2B_{2g}$	1.9797	0.0027		
		Radical Anion			
B_{3u}	$^2B_{3g} \rightarrow {}^2A_u$	0.8370	0.0102		
B_{3u}	$^2B_{3g} \rightarrow {}^2A_u$	1.5027	0.9716	1.41	11 356
B_{2u}	$^2B_{3g} \rightarrow {}^2B_{1u}$	1.5565	0.0253		
B_{2u}	$^2B_{3g} \rightarrow {}^2B_{1u}$	1.6552	0.0004		
B_{2u}	$^2B_{3g} \rightarrow {}^2B_{1u}$	2.1736	0.0034		

III.b.i. The Bright States. The experimental absorption spectrum of each neutral molecule and each molecular ion (cation and anion) is dominated by a strong absorption that is clearly reproduced by theory. In each case, the strong absorption has B_{3u} transition symmetry as shown in Tables 1−3. The transition symmetry is the product of the ground-state and excited-state symmetries. In other words, it is the representation of appropriate symmetry required to make the transition dipole moment totally symmetric. Therefore, it is necessarily the symmetry of the dipole operator that connects the ground state and excited state. We find that the designation of transition symmetries is particularly useful in our discussion of the bright states because while the type of transition is the same for each charge state (0, ±1) the actual ground- and excited-state symmetries are different.

The agreement of the strong absorption between experiment and calculation for each radical species is quite good, to within less than one or two tenths of an electronvolt. While the results calculated for the neutral are also qualitatively correct, TDDFT overestimates the strong B_{3u} transition by about one-third of an electronvolt for each neutral molecule. However, this is within the general accuracy of the method. This phenomenon of better TDDFT performance for radical absorptions than closed-shell absorptions presumably reflects limitations of the functionals and the adiabatic approximation and may merit a more complete study.

III.b.ii. Physical Interpretation of the Bright States. The general trend in the strong B_{3u} transition is that the neutral absorption is blue-shifted from the radical cation and radical anion absorption energies for a given molecular backbone. We may understand this energy trend by considering the orbitals involved in the transitions. To do this, we have performed attachment/detachment density analysis of the strong absorption for each of the three charge states of perylene. Attachment/detachment density plots show the electron density that moves during an electronic excitation.[15] The detachment and attachment densities represent the hole and particle densities, respectively. This analysis identifies which orbitals contribute most to the excitation, through the largest α and β electron eigenvalues of the transition.

The neutral system is closed-shell, and the calculation is performed with restricted orbitals, whereas the radical systems

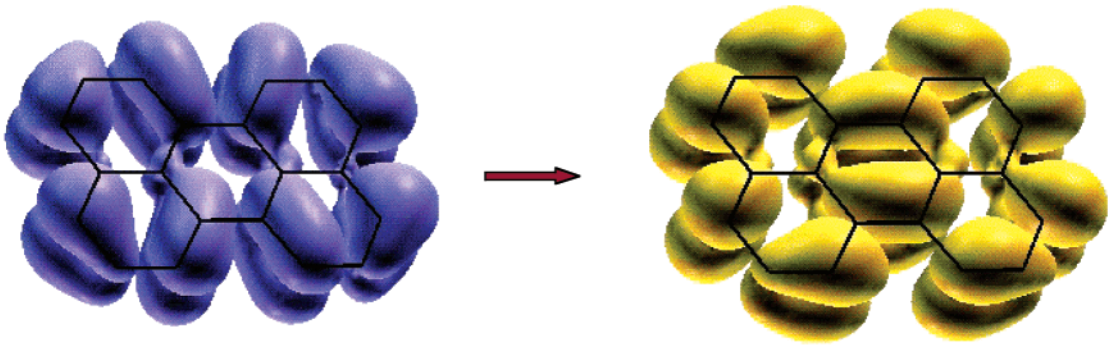

Figure 6. Neutral perylene BLYP/6-31G//BLYP/6-31G* attachment/detachment density of the $1^1A_g \rightarrow 1^1B_{3u}$ transition at 90% density enclosure. The left-hand plot shows the detachment density, which is removed from the ground state and rearranged as the attachment density (shown on the right) in the excited state.

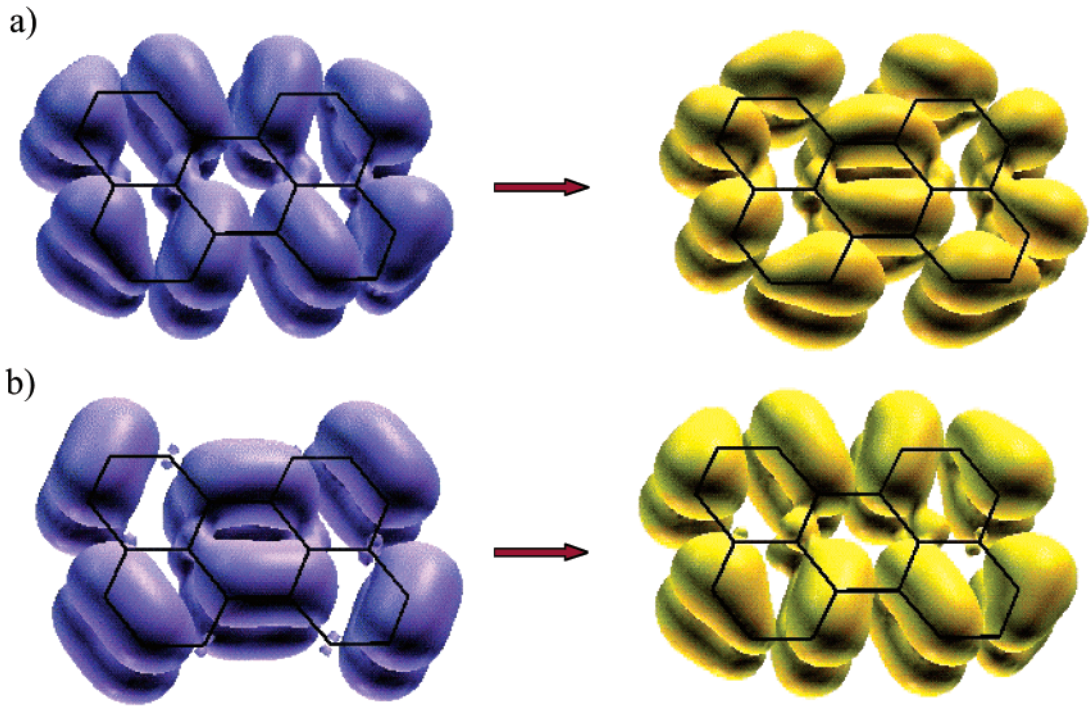

Figure 7. Perylene radical cation BLYP/6-31G//BLYP/6-31G* (a) α and (b) β electron attachment/detachment densities of the $1^2A_u \rightarrow 1^2B_{3g}$ transition at 90% density enclosure. See Figure 6 for further details.

TABLE 4: Attachment/Detachment Density Analysis of the Strong B_{3u} Absorption of the $C_{20}H_{12}$ Three Charge States[a]

$C_{20}H_{12}$ charge state	λ (A)$_\alpha$	λ (D)$_\alpha$	λ (A)$_\beta$	λ (D)$_\beta$
neutral	0.492	0.492	0.492	0.492
radical cation	0.443	0.443	0.538	0.538
radical anion	0.644	0.644	0.337	0.337

[a] Largest eigenvalues, λ, are given in units of electronic charge. Eigenvalues less than 0.1 e are omitted.

are open-shell, and the calculations are performed with unrestricted orbitals. The neutral transition appears to be a one-electron highest occupied molecular orbital (HOMO) to lowest unoccupied molecular orbital (LUMO) excitation. The radical transitions are also one-electron excitations; however, the total excitation is dominated by two configurations, which both involve changes in the occupation of the singly occupied molecular orbital (SOMO). We may confirm the identities of the orbitals involved in the transitions by attachment/detachment densities of the excitations.

Table 4 presents the largest α and β electron eigenvalues for the strong B_{3u} transition attachment/detachment density of the neutral, radical cation, and radical anion perylene. The neutral perylene α and β spin largest eigenvalues are identical because this is a closed-shell molecule. Because the eigenvalues are each approximately 0.5, the transition for this molecule is essentially described by a two-orbital, one-electron picture, in which the one electron may be α or β spin. The attachment/detachment density diagram for this transition is shown in Figure 6.

The cation and anion species are both radicals with unrestricted orbitals. This indicates that the SOMO, for example, may not be identical for the α and β electrons. As mentioned earlier, the strong absorption for both of these radicals involves contributions from movement in to and out of the singly occupied molecular orbital. We therefore need to consider both the α and β attachment/detachment densities separately. The α and β attachment/detachment densities are shown in Figures 7 and 8 for the radical cation and radical anion, respectively. The fact that there is movement in to and out of the SOMO indicates that these transitions are, at a minimum, described by a four-orbital picture.

The neutral excitation is a two-orbital, HOMO to LUMO transition. Comparing Figure 6 to Figures 7 and 8, it is possible to see that the radical cation α excitation is identical to the

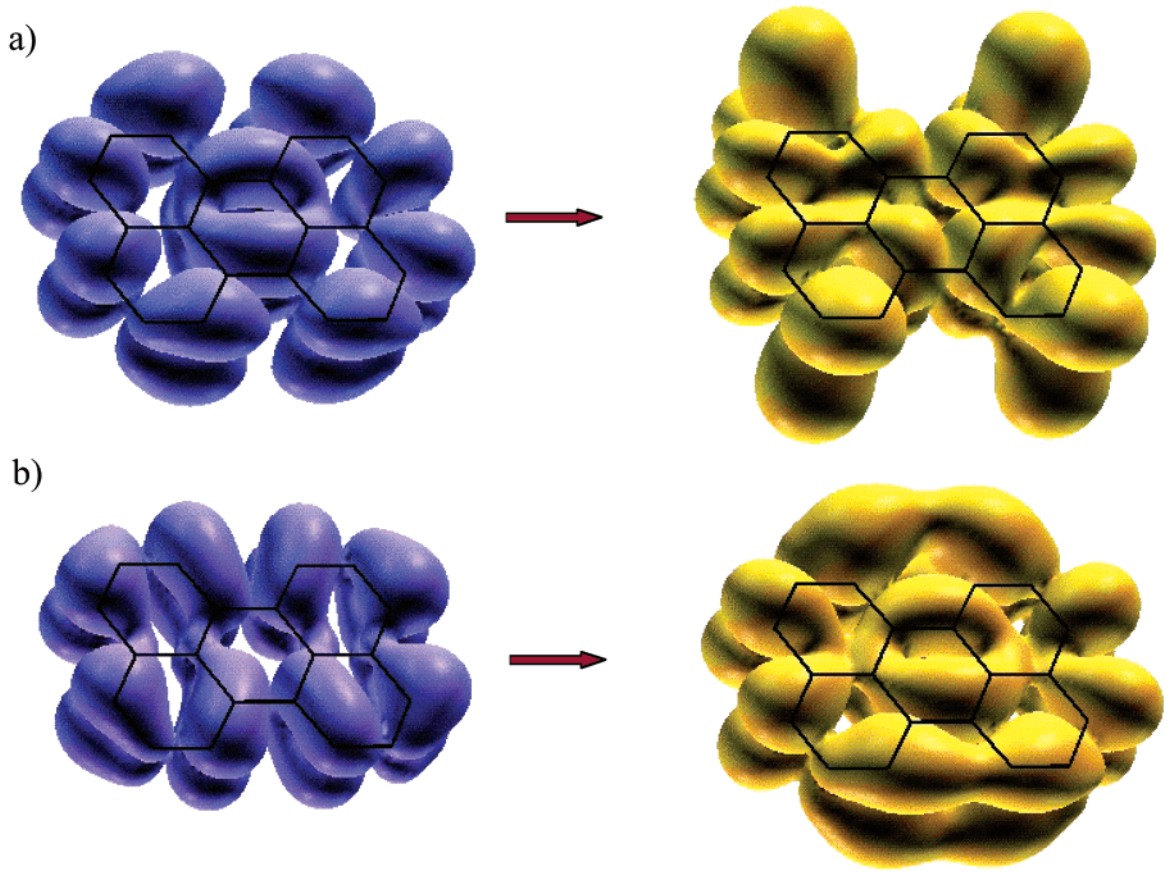

Figure 8. Perylene radical anion BLYP/6-31+G*//BLYP/6-31G* (a) α and (b) β electron attachment/detachment densities of the $1^2B_{3g} \rightarrow 1^2A_u$ transition at 90% density enclosure. See Figure 6 for further details.

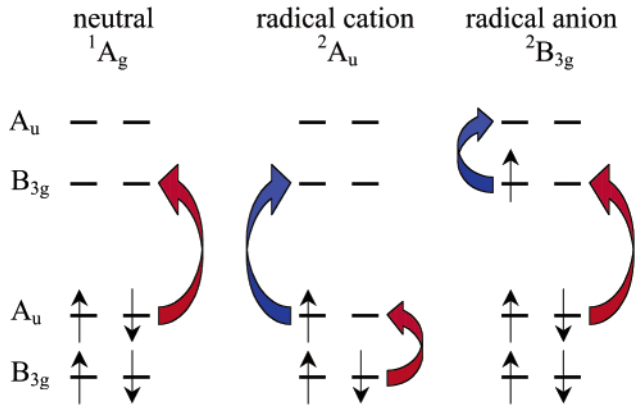

Figure 9. Schematic diagram of the neutral, radical cation, and radical anion strong B_{3u} transitions.

neutral excitation. This contribution to the radical cation transition is a HOMO to LUMO excitation in the α electron space. The radical anion β excitation is also essentially the same, only slightly more diffuse in character than the neutral and radical cation. This contribution to the radical anion transition is similarly a HOMO to LUMO excitation in the β electron space.

The radical cation and radical anion total excitations have contributions in both the α and β electron spaces. The contribution in the β space for the radical cation and α space for the radical anion are HOMO to LUMO excitations of appropriate symmetry to yield a B_{3u} transition. These then complete the four-orbital picture and are shown pictorially in Figure 9. Two orbitals are the HOMO and LUMO of the neutral excitation. The additional two orbitals come one each from the radical cation and radical anion excitations, the HOMO in the β space from the radical cation and the LUMO in the α space from the radical anion.

The two-orbital picture for the neutral transition and four-orbital picture for both radicals, as shown in Figure 9, explain the experimental blue shift of the neutral strong absorption. The neutral transition, as stated before, is a one-electron HOMO to LUMO excitation, as shown by a single red arrow. The radical transitions involve a superposition of two configurations, which together describe the total one-electron transition for each species. The two configurations are distinguished by two different colored arrows. Figure 9 shows α and β electrons being promoted for the radical transitions by arrows in blue and red, respectively. Each red arrow and each blue arrow depicts a one-electron transition from the ground-state configuration yielding an excitation of B_{3u} transition symmetry. There is configuration interaction between the one-electron excitations present in the radical transitions that lower their absorption energies from the neutral transition contribution. While TDDFT qualitatively predicts the blue shift for the neutral compounds relative to the cation and anion species, the quantitative accuracy for the shift is in poor agreement with experiment.

It is interesting to note that the red shift in the radical transitions could have been predicted very simply by Hückel molecular orbital (HMO) theory (for representative discussions, see ref 16). Because of particle−hole equivalence in the HMO model for alternate hydrocarbons, such as the molecules in the study, the energy differences between the HOMO and HOMO − 1 and LUMO and LUMO + 1 are identical. If we assume a configuration interaction picture in which the single excitation configurations of the lowest energy will interact, we should expect the same picture as we have seen described with TDDFT. In fact, also by particle−hole equivalence, HMO theory

with configuration interaction predicts *identical* excitation energies for the radical cation and radical anion species. This is not exactly what is observed experimentally, and this subtle difference in the cation and anion behavior (larger red shift for the anion) has been recovered with TDDFT.

III.b.iii. Astrophysical Implications of the Bright States. Some general astrophysical implications may be asserted from these results on the basis of the observed and calculated trends in the bright states. The perylene, terrylene, and quaterrylene series of strong B_{3u} transitions show definite trends in the excitation energies and oscillator strengths. The B_{3u} absorption has the same symmetry as the long axis of the molecule, as we will discuss further later, so perylene, terrylene, and quaterrylene can be related in terms of their long axis.

The trend in excitation energies for all three charge states is that the excitation energy decreases from perylene to terrylene to quaterrylene as follows from simple particle-in-a-box modeling. So, as the long axis of the molecule grows, the absorption energy decreases. This result is in excellent agreement with the semiempirical model developed by Salama et al.[2a] in their earlier discussion of the potential relation between neutral and ionized PAHs and the diffuse interstellar bands. On the other hand, the oscillator strength increases from perylene to terrylene to quaterrylene. As the molecule size increases, the intensity of the absorption does as well. Insight into this phenomenon may be gained by the transition density plots of the strong absorption within a set of charge state derivatives. We investigate the set of radical cations as an example of the general behavior of all three groups.

The perylene radical cation transition density is shown in Figure 10, at 90% density enclosure, along with the neutral and radical anion transition densities, to confirm that the radical cation is qualitatively representative of all three charge states. The positive and negative phases are shown in different colors. The contours are not opaque and so the darker regions are overlapping phases in one coordinate, although they do not occupy the same spatial density. Figure 10 shows that the general character of the transition density is the same for the neutral and radical species. It is possible to see from these plots that each transition density is characterized by a dipole moment along the long axis of the molecule.

This transition character is the same for all three radical cations, as seen in Figure 11. This then explains the growing oscillator strength with molecular size. Because the transition dipole is oriented along the long axis of the molecule, the dipole moment increases as the molecule length also increases on that axis. Therefore the intensity of this given absorption grows upon adding naphthalene units to the perylene backbone. We assert that the same type of transition character explains the oscillator strength trends in the neutral and radical anion species as well.

Physical interpretations of the transitions based on exciton theory are enlightening for these systems. We have already made reference to the growth pattern in perylene, terrylene, and quaterrylene as naphthalene unit additions, and this is the basis of an exciton theory analysis. Perylene may be treated as two interacting naphthalene units, terrylene as three interacting units, and quaterrylene as four. The long axis transition in perylene is then described by short axis transitions in the naphthalene units and the interaction between them. In this instance, experimental information about the short axis naphthalene transition and the long axis perylene transition determines the interaction energy necessary to be able to predict excitation energies and oscillator strengths for terrylene and larger oligorylene spectra based upon this mode of growth.

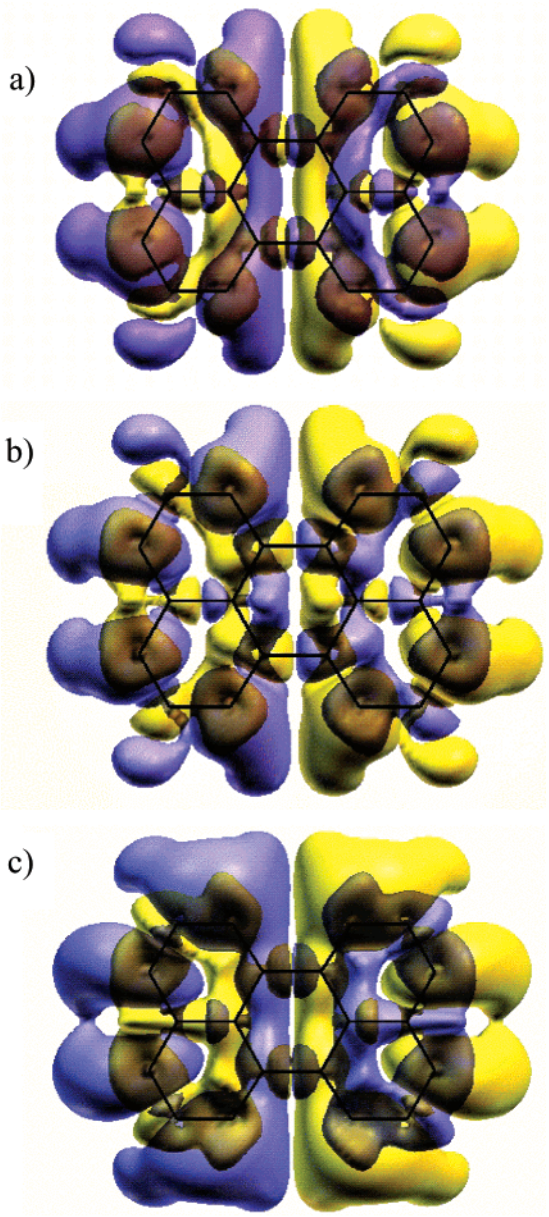

Figure 10. Perylene (a) radical cation, (b) neutral, and (c) radical anion strong absorption transition density at 90% density enclosure.

Using the experimental absorption energies for the short axis naphthalene transition, 4.45 eV,[17] and the long axis perylene transition, 2.96 eV, we then determine the interaction energy (V_{AB}) to be 1.49 eV. This subsequently leads to long axis transition energies of 2.34 and 2.04 eV for neutral terrylene and quaterrylene, respectively. These energies are in excellent agreement with experiment, 2.35 and 2.04 eV, respectively! We can also follow this same prescription, using TDDFT energies for naphthalene and perylene instead of experimentally determined energies. In this case, the exciton theory derived absorption energies for terrylene and quaterrylene match the calculated TDDFT energies. This indicates that exciton theory describes consistent behavior within the exact experimental framework and also the theoretical TDDFT framework.

The prediction of oscillator strengths ($f = {}^2/_3\omega|\breve{\mu}|^2$) based in exciton theory is not as satisfactory. The wave functions that are determined from exciton theory are based on nonoverlapping monomer wave functions. While the energies are explicitly dependent on an interaction energy term, the wave functions are independent of the interaction term. The transition moments

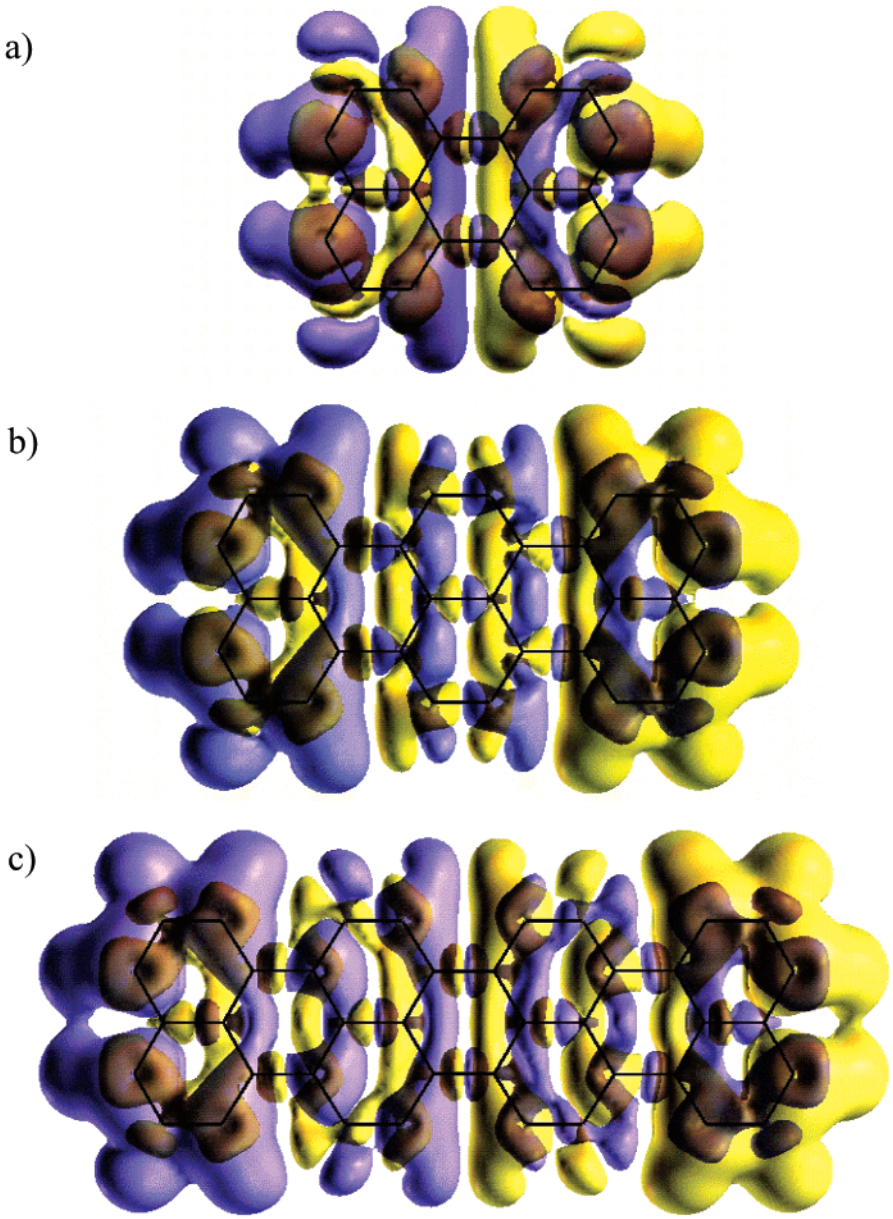

Figure 11. BLYP/6-31G//BLYP/6-31G* strong absorption transition density of (a) perylene cation, (b) terrylene cation, and (c) quaterrylene cation at 90% density enclosure.

for perylene, terrylene, and quaterrylene are then defined in terms of the transition moment of naphthalene. It is possible to show that the transition moments are exactly $1.414\mu_{\text{naphthalene}}$, $1.707\mu_{\text{naphthalene}}$, and $1.946\mu_{\text{naphthalene}}$ for perylene, terrylene, and quaterrylene, respectively. Given the TDDFT transition moment of naphthalene, $0.6625ea_0$, the perylene transition moment is predicted by exciton theory to be $0.9369ea_0$. However, the TDDFT transition moment of perylene is $2.1847ea_0$, which is far from the ideal (weakly coupled) value. By contrast, for two weakly interacting naphthalene molecules 10 Å apart, the transition moment to the allowed state is $0.9514ea_0$. Thus the simple exciton model does not adequately describe the strong increases in transition moment and oscillator strength seen in the electronic structure calculations.

The transition density plots suggest a simple model of transition dipole increasing linearly with addition of each naphthalene unit (from perylene to terrylene to quaterrylene) as the long axis length increases. Neglecting changes of excitation energy with increasing size, one would then predict oscillator strength growing quadratically with chain length and oscillator strength per unit mass of carbon growing linearly with chain length. The calculated results grow slightly less strongly than this (presumably because the above model overestimates charge separation and excitation energy decreases). It may, however, still be astrophysically significant that oscillator strength per unit mass increases as the oligorylene increases in size because this implies that larger PAHs of this type carry greater oscillator strength than is implied by simple molecular weight comparisons. Furthermore, a large size distribution is expected for interstellar PAHs that is expected to bridge the gap between the gas phase and the solid phase of interstellar dust.[2]

IV. Conclusions

We have presented experimental and theoretical absorption spectra of perylene, terrylene, and quaterrylene and their positive and negative ions. The oligorylenes isolated in Ne exhibit bright states in the visible region and thus imply possible associations with the diffuse interstellar bands.[2] These matrix-isolation results

motivate the further investigation of this subset of PAHs with gas-phase techniques.

Time-dependent density functional theory calculations predict absorption spectra in good agreement with the experimental results. The excitation energies and oscillator strengths of the B_{3u} bright states match well, especially for the radical species. The TDDFT calculations have allowed us to understand the character of the bright state transitions. The neutral excitations are shown to be single HOMO → LUMO transitions, while the radical excitations involve configuration interaction between promotions in to and out of the SOMO, leading to red shifts relative to the neutral.

For all neutral and radical species, the strong B_{3u} transition is the result of a transition dipole along the long axis of the molecule. The growth of the molecular backbone along the long axis of the molecule leads to a larger transition dipole moment for the bright state transition. In fact, the oscillator strength of the bright state per unit mass of carbon increases for larger oligorylenes, which may indicate a greater significance for these larger systems in relation to the DIBs and to the interstellar extinction curve in general. It would be interesting to determine a picture of the trends of the oscillator strength through further studies of other large PAH systems.

Acknowledgment. J.L.W. and M.H.G. thank the fellow authors for their invitation to collaborate on such an interesting study and also acknowledge support by the Director, Office of Energy Research, Office of Basic Energy Sciences, Chemical Sciences Division of the U.S. Department of Energy, under Contract No. DE-AC03-765F00098 and a grant from the Petroleum Research Fund. F.S. and T.M.H. acknowledge support from NASA, Office of Space Science, under Grant SARA 188-01-00-21 and the excellent technical support of R. Walker. The authors acknowledge many helpful discussions with Lou Allamandola.

Supporting Information Available: Tables 1−10 provide basis set effects on the calculations (Table 1) and vibronic transitions of neutral, anionic, and cationic perylene, terrylene, and quaterrylene. This material is available free of charge via the Internet at http://pubs.acs.org.

References and Notes

(1) (a) Allamandola, L. J.; Tielens, A. G. G. M.; Barker, J. R. *Astrophys. J. Suppl. Ser*. **1989**, *71*, 733. (b) Puget, J. L.; Léger, A. *Annu. Rev. Astron. Astrophys*. **1989**, *27*, 161. (c) Hudgins, D. M.; Allamandola, L. J. *Astrophys. J. Lett.* **1999**, *513*, L69.

(2) (a) Salama, F.; Bakes, E. L. O.; Allamandola, L. J.; Tielens, A. G. G. M. *Astrophys. J.* **1996**, *458*, 621. (b) Salama, F.; Galazutdinov, G. A.; Krelowski, J.; Allamandola, L. J.; Musaev, F. A. *Astrophys. J.* **1999**, *526*, 265.

(3) Ruiterkamp, R.; Halasinski, T.; Salama, F.; Foing, B.; Schmidt, W.; Ehrenfreund, P. *Astron. Astrophys*. **2002**, *390*, 1153.

(4) Halasinski, T. M.; Salama, F.; Allamandola, L. J. *Astrophys. J*., manuscript in preparation.

(5) Halasinski, T. M.; Hudgins, D. M.; Salama, F.; Allamandola, L. J.; Bally, T. *J. Phys. Chem. A* **2000**, *104*, 7484.

(6) (a) Runge, E.; Gross, E. *Phys. Rev. Lett*. **1984**, *52*, 997. (b) Petersilka, M.; Gossmann, U.; Gross, E. *Phys. Rev. Lett*. **1996**, *76*, 1212. (c) Bauernschmitt, R.; Alrichs, R. *Chem. Phys. Lett*. **1996**, *256*, 454.

(7) Hirata, S.; Lee, T.; Head-Gordon, M. *J. Chem. Phys*. **1999**, *111*, 8904.

(8) (a) Salama, F.; Allamandola, L. J. *J. Chem. Phys*. **1991**, *94*, 6964. (b) Salama, F.; Joblin, C.; Allamandola, L. J. *J. Chem. Phys*. **1994**, *101*, 10252.

(9) Becke, A. D. *Phys. Rev. A* **1988**, *38*, 3098.

(10) Lee, C.; Yang, W.; Parr, R. G. *Phys. Rev. B*, **1988**, *37*, 785.

(11) Kong, J.; White, C. A.; Krylov, A. I.; Sherrill, C. D.; Adamson, R. D.; Furlani, T. R.; Lee, M. S.; Lee, A. M.; Gwaltney, S. R.; Adams, T. R.; Ochsenfeld, C.; Gilbert, A. T. B.; Kedziora, G. S.; Rassolov, V. A.; Maurice, D. R.; Nair, N.; Shao, Y.; Besley, N. A.; Maslen, P. E.; Dombroski, J. P.; Dachsel, H.; Zhang, W. M.; Korambath, P. P.; Baker, J.; Byrd, E. F. C.; Van Voorhis, T.; Oumi, M.; Hirata, S.; Hsu, C. P.; Ishikawa, N.; Florian, J.; Warshel, A.; Johnson, B. G.; Gill, P. M. W.; Head-Gordon, M.; Pople, J. A. *J. Comput. Chem*. **2000**, *21*, 1532.

(12) (a) Szczepanski, J.; Chapo, C.; Vala, M. *Chem. Phys. Lett*. **1993**, *205*, 434. (b) Joblin, C.; Salama, F.; Allamandola, L. *J. Chem. Phys*. **1999**, *110*, 7287.

(13) (a) Joblin, C.; Salama, F.; Allamandola, L. *J. Chem. Phys*. **1995**, *102*, 9743. (b) Chillier, X. D. F.; Stone, B. M.; Salama, F.; Allamandola, L. J. *J. Chem. Phys*. **1999**, *111*, 449.

(14) Deperasinska, I.; Kozankiewicz, B.; Biktchantaev, I.; Sepiol, J. *J. Phys. Chem. A* **2001**, *105*, 810.

(15) Head-Gordon, M.; Grana, A. M.; Maurice, D.; White, C. A. *J. Phys. Chem*. **1995**, *99*, 14261.

(16) (a) Jaffé, H. H.; Orchin, M. *Theory and Applications of Ultraviolet Spectroscopy*; John Wiley and Sons: New York, 1962. (b) Murrel, J. N. *The Theory of the Electronic Spectra of Organic Molecules*; Spottiswoode, Ballantyne & Co. Ltd.: London, 1963.

(17) George, G. A.; Morris, G. C. *J. Mol. Spectrosc.* **1968**, *26*, 67.